Int. J. Heat Mass Transfer. Vol. 36, No. 5, pp. 1251–1259, 1993
Printed in Great Britain

0017-9310/93 $6.00 + 0.00


# Bench mark solutions to natural convection heat transfer problem around a horizontal circular cylinder

T. SAITOH,† T. SAJIKI‡ and K. MARUHARA†

† Department of Aeronautics and Space Engineering, Tohoku University, Sendai 980, Japan
‡ Toyota Motors Corporation, Toyota 471, Japan

(*Received* 19 *May* 1992)

**Abstract**—High-accuracy bench mark solutions are presented for the natural convection flow around a horizontal circular cylinder with uniform surface temperature. In the past two decades, several approximate and numerical solutions to this problem have been reported in the literature. However, owing to limitations of (i) computer running time (CPU time) and (ii) resolution of the solution methodology, no exact bench mark solution has been presented to date. A large computational domain is inevitably necessitated in the case of small Rayleigh numbers. A thin boundary layer forms when the Rayleigh number increases, thereby requiring high resolution in the vicinity of the cylinder surface. Both of these features make it difficult to obtain exact bench mark solutions. These difficulties were overcome by adopting a high-accuracy fourth-order finite difference method and a coordinate transformation technique. The present bench mark solutions are accurate to at least three decimal places for small Rayleigh numbers (e.g. $Ra = 10^3$ and $10^4$) and will be quite useful as standard comparison solutions to which many numerical solutions can be compared. Further, typical isotherms, streamlines, vorticities, local Nusselt numbers, tangential and radial velocities and temperature distributions were clarified in detail.

## 1. INTRODUCTION

NATURAL convection around a horizontal circular cylinder under constant temperature or constant heat flux conditions in an infinite fluid space has recently attracted much attention [1–3]. This problem is of importance not only in practical heat transfer equipment but also in that it poses a standard heat transfer problem which can be regarded as a bench mark solution to validate numerical methodologies of various kinds.

In the past decade, extensive studies on natural convection flow about a horizontal circular cylinder have been presented. Kuehn and Goldstein [1] have solved the full Navier–Stokes and energy equations for natural convection around an isothermal circular cylinder over a wide range of Rayleigh numbers from $10^0$ to $10^7$ using a finite difference scheme. They used neither the boundary layer approximation nor a curvilinear coordinate system. They presented the local and average Nusselt numbers for a wide variety of the Rayleigh and the Prandtl numbers with experimental data using a Mach–Zehnder interferometer.

The inflow and outflow boundary conditions were imposed at the artificially placed outer boundary. These conditions may be valid only in the steady state condition, as discussed in Wang *et al.*'s paper [3].

Just after Kuehn and Goldstein's work, Fujii *et al.* [4] presented theoretical and experimental results on natural convection heat transfer about a horizontal wire. They used two computational domains: one is a domain near the cylinder prescribed by a cylindrical coordinate system and the other is one outside this domain prescribed by a rectangular coordinate system. The inner boundary was located at $r_c = 40r_0$, $r_0$ being the cylinder diameter. The vertical outer edge was positioned to be $170r_0$. They utilized two outer boundary conditions: an open boundary condition and a solid boundary condition in order to check the validity of the boundary conditions. Although they did not present the numerical results for relatively large Rayleigh numbers (i.e. $Ra = 10^3$–$10^5$), it seems to the present authors that their results for $Ra = 0.37$ are quite accurate and reliable even now. In this sense, their paper is the best of those in the last two decades.

Recently, Wang *et al.* [3] solved the same problem as the one treated by Kuehn and Goldstein. Necessarily, the governing equations and the boundary conditions including inflow and outflow conditions at the outer imaginary boundary were exactly the same.

The numerical methodology used in their computations was the spline fractional step method (SFSM), which they claim can achieve more accurate solutions than existing finite difference methods using fewer grid points, resulting in a considerable saving in computer memory requirements. They also presented the numerical results for (i) uniform surface heat flux and (ii) mixed boundary conditions other than isothermal surface conditions.

Wang *et al.* also made a comparison between their numerical results and those obtained by Kuehn and Goldstein under an isothermal surface boundary condition for different Rayleigh numbers and found a good agreement with their results. The maximum

## NOMENCLATURE

| | |
|---|---|
| $a$ | thermal diffusivity |
| $D$ | cylinder diameter |
| $Fo$ | Fourier number, $at/D^2$ |
| $g$ | gravitational acceleration |
| $Gr$ | Grashof number, $g\beta\Delta TD^3/v^2$ |
| $h$ | $\Delta x$ |
| $h_a$ | local heat transfer coefficient |
| $\overline{h_a}$ | average heat transfer coefficient around cylinder |
| $k$ | thermal conductivity of fluid or time step ($\Delta t$) |
| $L$ | radial distance between cylinder surface and outer boundary of solution domain |
| $M, N$ | number of mesh points in $r$ and $\theta$ directions, respectively |
| $Nu$ | local Nusselt number, $h_aD/k$ |
| $\overline{Nu}$ | average Nusselt number |
| $Pr$ | Prandtl number, $v/a$ |
| $r$ | radial coordinate |
| $Ra$ | Rayleigh number, $Pr\,Gr$ |
| $t$ | dimensionless time, $t'\alpha/D^2$ |
| $t'$ | time |
| $\Delta t$ | time step |
| $T$ | dimensionless temperature, $(T-T_\infty)/(T_w-T_\infty)$ |
| $T_w$ | temperature of cylinder surface |
| $T_\infty$ | temperature of ambient fluid |
| $\Delta T$ | $T_w-T_\infty$ |
| $u$ | dimensionless radial velocity, $UD/\alpha$ |
| $U$ | radial velocity |
| $v$ | dimensionless angular velocity, $VD/\alpha$ |
| $V$ | angular velocity |
| $\Delta x, \Delta y$ | mesh length in $x$ and $y$ directions, respectively |
| $Y$ | radial distance from cylinder surface |
| $Y^*$ | $Y\,Ra^{1/4}/D$. |

Greek symbols

| | |
|---|---|
| $\alpha$ | thermal diffusivity |
| $\beta$ | coefficient of thermal expansion |
| $\theta$ | angular coordinate; zero is downward vertical positive counterclockwise on right half of cylinder |
| $v$ | kinematic viscosity |
| $\psi$ | dimensionless stream function |
| $\Delta\psi$ | difference between neighboring streamlines |
| $\omega$ | dimensionless vorticity. |

Subscripts

| | |
|---|---|
| $i,j$ | nodal position in radial and angular directions, respectively |
| max | maximum value |
| min | minimum value. |

deviation between the two solutions was 1.6%. Other recent studies [1–3] were also introduced in Wang *et al.*'s paper.

However, the inflow and outflow conditions used by Kuehn and Goldstein and Wang *et al.* do not give the correct results including streamlines and the Nusselt number around the cylinder. The only exceptional study is the one by Fujii *et al.*, previously introduced. However, to date, no exact bench mark solution for this standard comparison problem to which various numerical solutions are to be compared has been given in the literature. It seems that even the two solutions (i.e. Kuehn–Goldstein and Wang *et al.*) introduced above contain errors of more than 2%, so that the two numerical solutions cannot be regarded as the standard bench mark solutions. Bench mark solutions to natural convection flow in a square channel with two hot and cold vertical and two adiabatic horizontal boundaries have already been obtained by Saitoh and Hirose [5] (up to four significant figures) and de Vahl Davis [6] (up to two significant figures).

Motivated mainly by the above circumstances, we aim to find the bench mark solutions for the natural convection heat transfer problem around a horizontal circular cylinder under isothermal conditions. In order to make verification of the computed results, five different kinds of numerical methodologies have been used in the present work:

(i) the ordinary explicit finite difference method (FDM);
(ii) the multi-point FDM with uniform mesh of order $O(\Delta r^4)$ with $\Delta r$ being the spatial mesh length;
(iii) the multi-point FDM with two computation domains;
(iv) the multi-point FDM with logarithmic coordinate transformation;
(v) the multi-point FDM with logarithmic coordinate transformation and a solid boundary condition.

In the last scheme, we adopted the solid boundary condition as the outer boundary condition (see Fig. 1) in order to eliminate an ambiguity of the outer boundary. The solid boundary condition was placed at some 1000–20 000 times the cylinder diameter, depending on the Rayleigh number. The computational domain has a key influence on the flow patterns and the Nusselt number distributions around the cylinder. First, we will show the governing equations with the boundary conditions, then numerical methods and,

finally, numerical results via the various methods mentioned above.

The present bench mark solutions are accurate to at least three decimal places for Rayleigh numbers (ranging from $Ra = 10^3$ to $10^5$), and will be quite useful as standard comparison solutions to which many numerical solutions can be compared.

Further, typical isotherms, streamlines, vorticities, local Nusselt numbers, tangential and radial velocities and temperature distributions around the cylinder are clarified in detail.

## 2. GOVERNING EQUATIONS

Figure 1 shows the geometry of interest with cylindrical polar coordinates. The dimensionless Navier–Stokes and energy equations for steady, laminar natural convection flow may be written under the Boussinesq approximation as follows:

$$\frac{\partial T}{\partial t} = -u\frac{\partial T}{\partial r} - \frac{v}{r}\frac{\partial T}{\partial \theta} + \nabla^2 T \tag{1}$$

$$\frac{\partial \omega}{\partial t} = -u\frac{\partial \omega}{\partial r} - \frac{v}{r}\frac{\partial \omega}{\partial \theta} + Pr\nabla^2\omega + Ra\,Pr\left(\sin\theta\frac{\partial T}{\partial r} + \frac{\cos\theta}{r}\frac{\partial T}{\partial \theta}\right) \tag{2}$$

$$\omega = -\nabla^2\psi \tag{3}$$

with Laplacian $\nabla^2$

$$\nabla^2 \equiv \frac{\partial^2}{\partial r^2} + \frac{1}{r}\frac{\partial}{\partial r} + \frac{1}{r^2}\frac{\partial^2}{\partial \theta^2} \tag{4}$$

and the stream function $\psi$

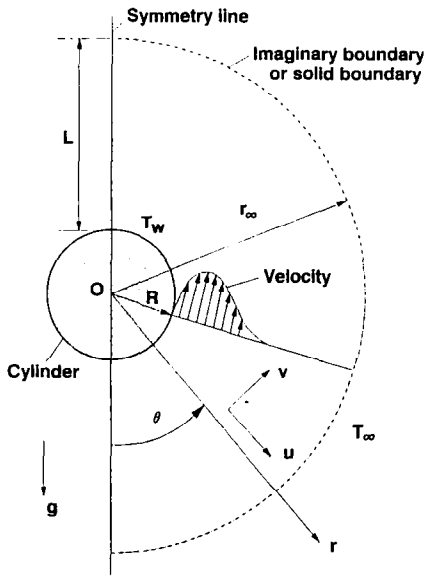


FIG. 1. Schematic model and coordinate system for steady laminar natural convection around a horizontal isothermal circular cylinder.

$$u = \frac{1}{r}\frac{\partial \psi}{\partial \theta}, \quad v = -\frac{\partial \psi}{\partial r}. \tag{5}$$

Only half the domain was solved as the flow is symmetrical about the vertical plane, including the cylinder axis.

The boundary conditions are

on the isothermal cylinder surface:

$$u = v = \psi = 0, \quad \omega = -\frac{\partial^2 \psi}{\partial r^2}, \quad T = 1; \tag{6}$$

on the symmetry lines:

$$v = \psi = \omega = \frac{\partial u}{\partial \theta} = \frac{\partial T}{\partial \theta} = 0. \tag{7}$$

As for the outer boundary conditions, we adopted the following two kinds of conditions

(a) inflow and outflow condition:

at the inflow region

$$v = \frac{\partial^2 \psi}{\partial r^2} = T = 0, \quad \omega = -\frac{1}{r^2}\frac{\partial^2 \psi}{\partial \theta^2}; \tag{8}$$

at the outflow region

$$v = \frac{\partial^2 \psi}{\partial r^2} = \frac{\partial T}{\partial r} = 0, \quad \omega = -\frac{1}{r^2}\frac{\partial^2 \psi}{\partial \theta^2}; \tag{9}$$

(b) solid boundary condition (methodology (v)):

$$v = u = \psi = T = 0, \quad \omega = -\frac{\partial^2 \psi}{\partial r^2}. \tag{10}$$

The inflow–outflow condition has the same outer boundary conditions as in the paper of Kuehn and Goldstein. In this case, two boundary conditions are given at the artificial boundary according to the inflow and outflow situation. The point of maximum stream function is selected as the boundary splitting inflow and outflow. However, this inflow–outflow condition gives a considerable error, especially when the Rayleigh number is small.

*Coordinate transformation*

In order to implement computation in a wide domain subject to the solid boundary condition mentioned above, it is desirable to perform a coordinate transformation. Such a coordinate transformation technique is also necessary to improve the resolution of the solution near the cylinder surface. In this study, we utilized a logarithmic coordinate transformation

$$\eta = \ln r. \tag{11}$$

By virtue of this transformation, the resultant governing equations can be written as follows:

$$\frac{\partial T}{\partial t} = -\frac{u}{r}\frac{\partial T}{\partial \eta} - \frac{v}{r}\frac{\partial T}{\partial \theta} + \nabla^2 T \tag{12}$$

$$\frac{\partial \omega}{\partial t} = -\frac{u}{r}\frac{\partial \omega}{\partial \eta} - \frac{v}{r}\frac{\partial \omega}{\partial \theta} + Pr\nabla^2\omega + Pr\,Ra\left(\frac{\sin\theta}{r}\frac{\partial T}{\partial \eta} + \frac{\cos\theta}{r}\frac{\partial T}{\partial \theta}\right) \quad (13)$$

$$\omega = -\nabla^2\psi \quad (14)$$

with Laplacian $\nabla^2$

$$\nabla^2 \equiv \frac{1}{r^2}\left(\frac{\partial^2}{\partial \eta^2} + \frac{\partial^2}{\partial \theta^2}\right) \quad (15)$$

and the stream function $\psi$

$$u = \frac{1}{r}\frac{\partial \psi}{\partial \theta}, \quad v = -\frac{1}{r}\frac{\partial \psi}{\partial \eta}. \quad (16)$$

Of course, $r$ is given by

$$r = \exp \eta. \quad (17)$$

## 3. METHOD OF SOLUTION

In order to check and validate the proposed bench mark solutions (BMSs), we used five kinds of solution approaches using two kinds of finite difference methods:

(i) explicit FDM with uniform grids (EX-1);
(ii) multi-point FDM with uniform grids (ME-1);
(iii) multi-point FDM with two computational domains (ME-2);
(iv) multi-point FDM with logarithmic transformation (ME-3);
(v) multi-point FDM with logarithmic transformation and solid boundary condition (ME-4).

The above five schemes are listed in Table 1 with the degree of accuracy. Schemes (ii), (iii), (iv) and (v) have a degree of accuracy of fourth-order $O(h^4)$, with $h$ being the mesh length.

In order to cope with the high Rayleigh number problem under moderate cost performance and allowable accuracy, two major tools are used, i.e. a high-degree-of-accuracy finite difference scheme and coordinate transformation. These are indispensable factors when dealing with multi-dimensional, especially three-dimensional, problems since the computer running time (CPU time) is roughly proportional to $h^{n+2}$, $n$ being the number of dimensions. Therefore, to decrease the CPU time, it is most effective to use a coarse mesh length. However, this will result in considerable degradation of resolution of the numerical results.

Generally speaking, the following three considerations, including numerical methods and techniques, are required to obtain accurate and reliable bench mark solutions:

(i) numerical methodology, for example fourth-order FDM;
(ii) coordinate transformation, which is efficacious to improve high resolution near the cylinder and to cover a wide computational domain;
(iii) outer boundary condition; for example, the inflow–outflow condition or the solid boundary condition.

*Multi-point finite difference scheme*

The multi-point explicit finite difference method (MEFDM) was first presented by Saitoh. Four multi-point schemes, i.e. multi-point explicit, multi-point implicit, multi-point Adams–Bashforth, and multi-point DuFort–Frankel, have been proposed.

The multi-point approximations of the first and second derivatives, for example, are described as follows:

$$\left.\frac{\partial u}{\partial x}\right|_{i,j} = \frac{u_{i-2} - 8u_{i-1} + 8u_{i+1} - u_{i+2}}{12h} + \frac{4}{5!}h^4\frac{\partial^6 u}{\partial x^6}\cdots \quad (18)$$

Table 1. Five finite difference schemes with grid fineness, degree of accuracy and computation domain to obtain bench mark solutions

| | Abbreviations | FDM | Grids ($M \times N$) | Degree of accuracy | Computation domain, $L$ | B.C. | Remarks |
|---|---|---|---|---|---|---|---|
| (i) | EX-1 | Explicit | uniform ($120 \times 72$) | $O(h^2)$ | 1.5–3 | inflow and outflow | $h$: mesh length |
| (ii) | ME-1 | Multi-point [5] | uniform ($120 \times 72$) | $O(h^4)$ | 1.5–3 | inflow and outflow | |
| (iii) | ME-2 | Multi-point | two different grids ($h_1$, $h_2$) ($50 \times 72$), ($50 \times 72$) | $O(h_1^4)$ | 3–8 | inflow and outflow | $h_1 > h_2$ |
| (iv) | ME-3 | Multi-point | logarithmic transformation $X = \ln(r)$ ($120 \times 72$) | $O(h^4)$ | 5–12 | inflow and outflow | |
| (v) | ME-4 | Multi-point | logarithmic transformation $X = \ln(r)$ ($120 \times 72$), ($300 \times 144$) | $O(h^4)$ | 1000–20 000 | solid | |

B.C., outer boundary condition.

$$\left.\frac{\partial^2 u}{\partial x^2}\right|_{i,j} = \frac{-u_{i-2}+16u_{i-1}-30u_i+16u_{i+1}-u_{i+2}}{12h^2} + \frac{8}{6!}h^4\frac{\partial^6 u}{\partial x^6}\cdots \quad (19)$$

The above central difference was used for the advection terms of the Navier–Stokes equations. The truncation error $T_{i,j}$ of the MEFDM for the one-dimensional heat conduction equation is given by

$$T_{i,j} = \frac{u_{i,j+1}-u_{i,j}}{k} - \frac{-u_{i-2,j}+16u_{i-1,j}-30u_{i,j}+16u_{i+1,j}-u_{i+2,j}}{12h^2} - \left(\frac{\partial u}{\partial t}-\frac{\partial^2 u}{\partial x^2}\right)_{i,j} = \frac{k}{2}\frac{\partial^2 u}{\partial t^2}+\frac{h^4}{90}\frac{\partial^6 u}{\partial x^6}+\frac{k^2}{6}\frac{\partial^3 u}{\partial t^3} + \frac{h^6}{1008}\frac{\partial^8 u}{\partial x^8}+\cdots \quad (20)$$

The stability range of the MEFDM is prescribed by

$$\frac{k}{h^2} \leqslant \frac{3}{8} \quad (21)$$

for the one-dimensional heat conduction equation.

It is important that all boundary conditions are expressed by the fully fourth-order equations. For example, the fully fourth-order expressions for the typical boundary conditions are shown below

(i) adiabatic condition

$$u_{i-1,j} = u_{i+1,j};\ u_{i-2,j} = u_{i+2,j};$$

(ii) constant temperature condition ($u_{i,j} = C$)

$$u_{i,j} = C;\ u_{i-1,j} = 2C - u_{i+1,j};$$

(iii) vorticity at the wall in Poisson's equation

$$\omega_{i,j} = \nabla^2\psi \text{ when } \psi_{i,j} = \left.\frac{\partial\psi}{\partial x}\right|_i = 0$$

$$\omega_{i,j} = \frac{1}{(\Delta x)^2}\{\tfrac{1}{8}\psi_{i+1,j}-3\psi_{i+2,j}+\tfrac{8}{9}\psi_{i+3,j} - \tfrac{1}{8}\psi_{i+4,j}\}$$

$$\omega_{i-1,j} = 6\omega_{i,j}-15\omega_{i+1,j}+20\omega_{i+2,j}-15\omega_{i+3,j} + 6\omega_{i+4,j}-\omega_{i+5,j}.$$

The mesh length, computational domain (distance between cylinder surface and imaginary boundary) and the time step for typical Rayleigh number are listed in Table 1. In the two-uniform grid computation, two different grids were used in order to raise the degree of accuracy in the vicinity of the cylinder, i.e. the finer mesh was employed for the inner domain near the cylinder surface.

One typical feature of the natural convection flow around a horizontal circular cylinder over a wide range of Rayleigh numbers is that the computational domain extends a considerable distance from the cylinder surface, especially when the Rayleigh number is small.

So, it is quite efficient if a coordinate transformation such as logarithmic transformation is adopted. The grid size near the cylinder surface will be only 1/60 to 1/80 of the cylinder radius, thereby assuring the degree of accuracy. Further, the computation domain can be enlarged to 1000–20 000 times as wide as the cylinder radius.

The computer running time for a typical parameter set ($\Delta t = 10^{-4}$, $M = 120$, $N = 72$) was some $3 \times 10^5$ s on a Data General AV-300.

## 4. BENCH MARK SOLUTIONS AND OTHER COMPUTED RESULTS

Numerical calculations were carried out for an isothermal circular cylinder with fixed Prandtl number $Pr = 0.7$ and Rayleigh numbers ranging from $Ra = 10^3$ to $10^5$. Typical computed results for streamlines, isotherms, vorticities and tangential velocity distributions are shown in Figs. 2–5 with different Rayleigh numbers. As indicated in the previous studies, the boundary layer becomes thin with increasing Rayleigh number. These results have been obtained by using methodology (v) and only the vicinity near the cylinder was enlarged.

Time sequences of isotherms and streamlines are designated in Fig. 6. It is seen that the heated fluid ascends with formation of a heated cap. This heated cap eventually approaches the solid boundary, which is an artificial boundary, and disappears in the vicinity of the solid boundary.

While the center of the vortex is initially formed very near the cylinder, it moves upwards with elapse of time and stays at a certain position. Then a steady state condition will prevail at this time point. In order to avert an influence of the existence of the solid boundary on the free flow pattern, the solid boundary should be placed 200–500 times further away from the cylinder diameter. As seen from Fig. 2(a), the solid boundary placed at about $700D$ has no influence on the heat transfer characteristics in the steady state condition.

A comparison between the present numerical solution and that of Fujii *et al.* for $Pr = 0.7$ and $Ra = 0.37$ is shown in Fig. 7. The present results are in good agreement with their numerical results at peripheral angles of 0–60°, and after that, with their experimental results. It is especially noted here that Fujii *et al.*'s results can be judged to be quite excellent since their results were obtained as early as 1982.

The Nusselt number profiles of four different research groups are shown in Fig. 8 for $Pr = 0.7$ and $Ra = 10^4$. Five numerical results, including the present bench mark solutions, are compared in the figure. It is quite surprising to see the large discrepancies among the four numerical results. The principal cause of this discrepancy lies in the fineness of the grid

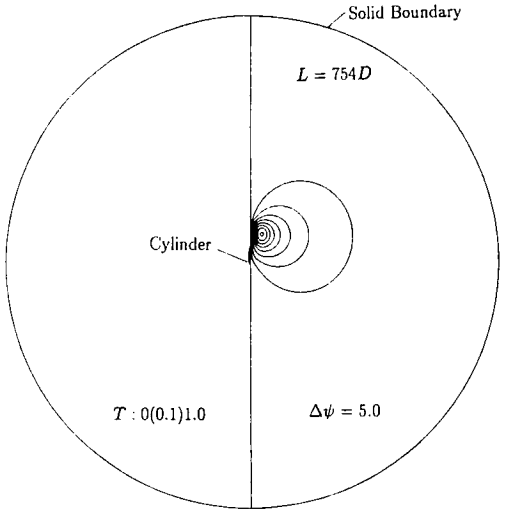


FIG. 2(a). Computed isotherms and streamlines for $Ra = 0.37$ and $Pr = 0.7$.

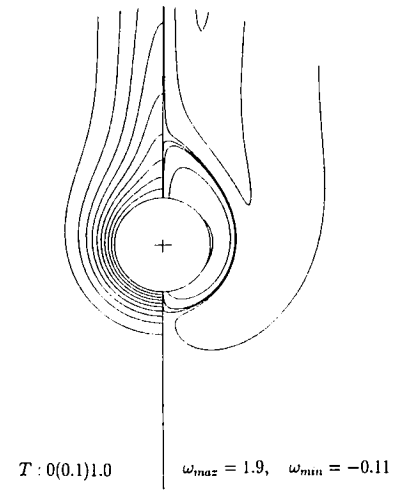


FIG. 3(a). Computed isotherms and vorticities for $Ra = 10^3$ and $Pr = 0.7$.

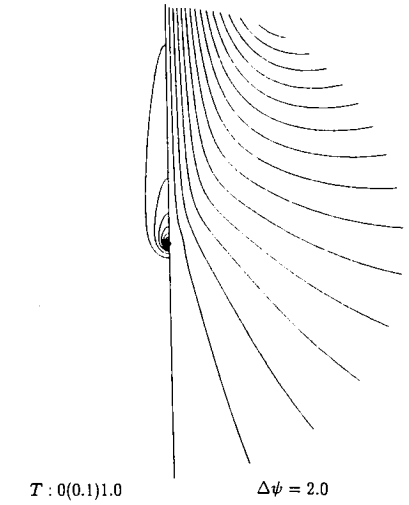


FIG. 2(b). Computed isotherms and streamlines for $Ra = 0.37$ and $Pr = 0.7$.

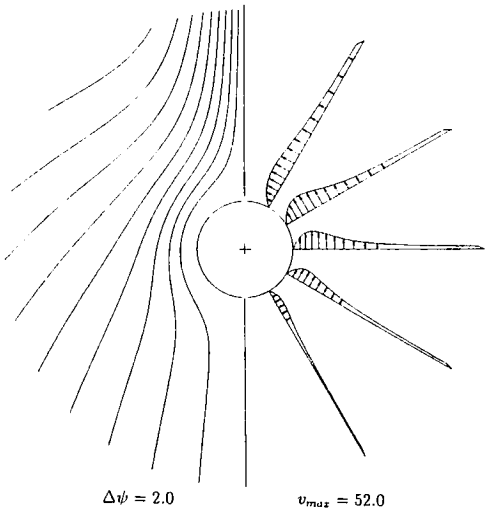


FIG. 3(b). Computed streamlines and tangential velocity distribution for $Ra = 10^3$ and $Pr = 0.7$.

spacing used and the width of the computation domain. In our present analysis, the high-accuracy fourth-order FDM was adopted and the computation domain was also enlarged to 700–2000 times the cylinder radius by introducing a logarithmic coordinate transformation.

Figure 9 shows a comparison between the present BMSs and the experimental data of Didion and Oh

Table 2. Comparison of the present bench mark solutions with the results of Kuehn–Goldstein and Wang *et al.* for $Ra = 10^3$, $10^4$ and $10^5$

| $Ra$ | | $Nu$ | | | | | | | |
|---|---|---|---|---|---|---|---|---|---|
| | | $\theta = 0°$ | 30° | 60° | 90° | 120° | 150° | 180° | $\overline{Nu}$ |
| $10^3$ | Present | 3.813 | 3.772 | 3.640 | 3.374 | 2.866 | 1.975 | 1.218 | 3.024 |
| | Kuehn and Goldstein [1] | 3.89 | 3.85 | 3.72 | 3.45 | 2.93 | 2.01 | 1.22 | 3.09 |
| | Wang *et al.* [3] | 3.86 | 3.82 | 3.70 | 3.45 | 2.93 | 1.98 | 1.20 | 3.06 |
| $10^4$ | Present | 5.995 | 5.935 | 5.750 | 5.410 | 4.764 | 3.308 | 1.534 | 4.826 |
| | Kuehn and Goldstein [1] | 6.24 | 6.19 | 6.01 | 5.64 | 4.82 | 3.14 | 1.46 | 4.94 |
| | Wang *et al.* [3] | 6.03 | 5.98 | 5.80 | 5.56 | 4.87 | 3.32 | 1.50 | 4.86 |
| $10^5$ | Present | 9.675 | 9.557 | 9.278 | 8.765 | 7.946 | 5.891 | 1.987 | 7.898 |
| | Kuehn and Goldstein [1] | 10.15 | 10.03 | 9.65 | 9.02 | 7.91 | 5.29 | 1.72 | 8.00 |
| | Wang *et al.* [3] | 9.80 | 9.69 | 9.48 | 8.90 | 8.00 | 5.80 | 1.94 | 7.97 |

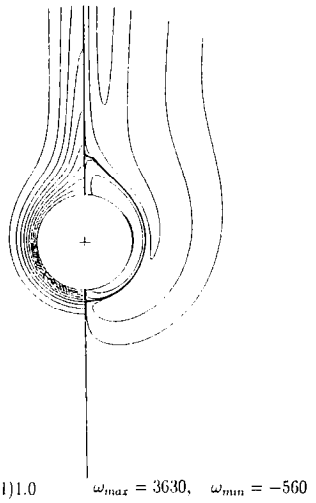


FIG. 4(a). Computed isotherms and vorticities for $Ra = 10^4$ and $Pr = 0.7$.

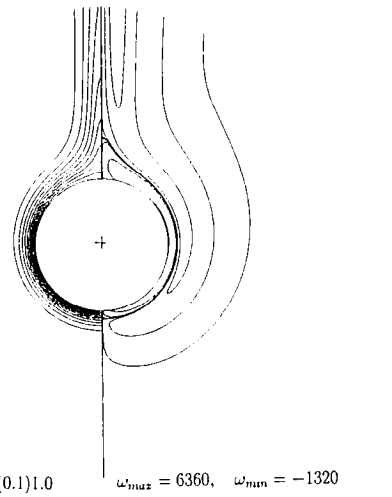


FIG. 5(a). Computed isotherms and vorticities for $Ra = 10^5$ and $Pr = 0.7$.

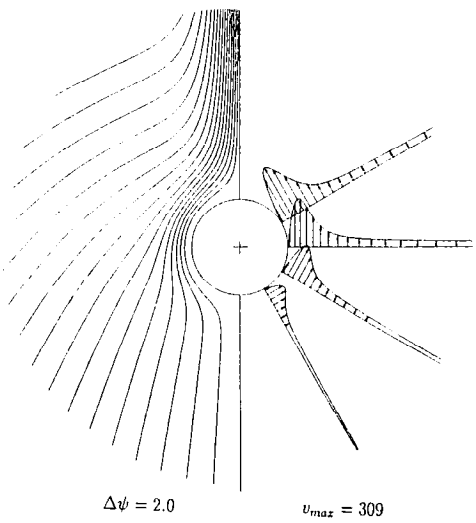


FIG. 4(b). Computed streamlines and tangential velocity distribution for $Ra = 10^4$ and $Pr = 0.7$.

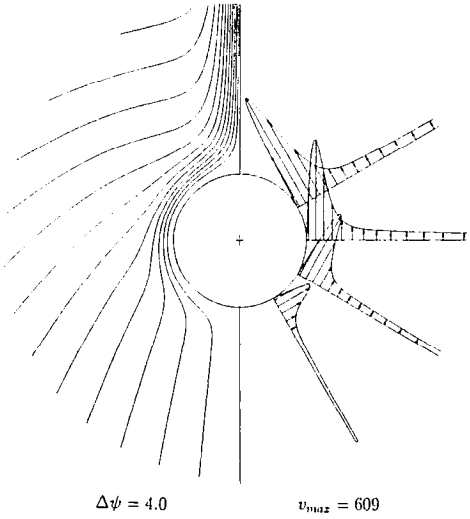


FIG. 5(b). Computed streamlines and tangential velocity distribution for $Ra = 10^5$ and $Pr = 0.7$.

[7], Eckert and Soehngen [8], and, Kuehn and Goldstein [1] for $Ra = 10^5$. Although the present results are slightly lower than the experimental data, the cause of the difference cannot be attributed to the error of computation as the measurement contains significant error.

The present bench mark solutions are listed in Table 2 together with the results of Kuehn–Goldstein and Wang *et al.* The grid sizes (radial and peripheral), computation domain $L$, and other conditions used for the present calculation are listed separately in Table 1.

Further, the numerical results by using five schemes are compared in Table 3. This comparison gives strong evidence that the present BMSs are correct, at least to three decimal places. Comparison of the present BMS with the other two numerical results (Table 2) clearly shows that there is a large difference at $\theta = 0°$, i.e. at the lower stagnation point.

It is quite difficult to obtain high-accuracy bench mark solutions even for such a simple geometry as is treated in this paper. The computer running time and core memory prevent one from obtaining accurate BMSs if the ordinary three-point FDMs of order $O(h^2)$ are used.

In this sense, the numerical methodologies presented here to obtain BMSs are marked features of high efficiency using scaled grid spacing and high truncation error of order $O(h^4)$. These features are indispensable in order to obtain the BMSs.

Further, it is noted here that we have performed an additional numerical computation using a variable mesh finite difference scheme and obtained the same results as introduced in this paper.

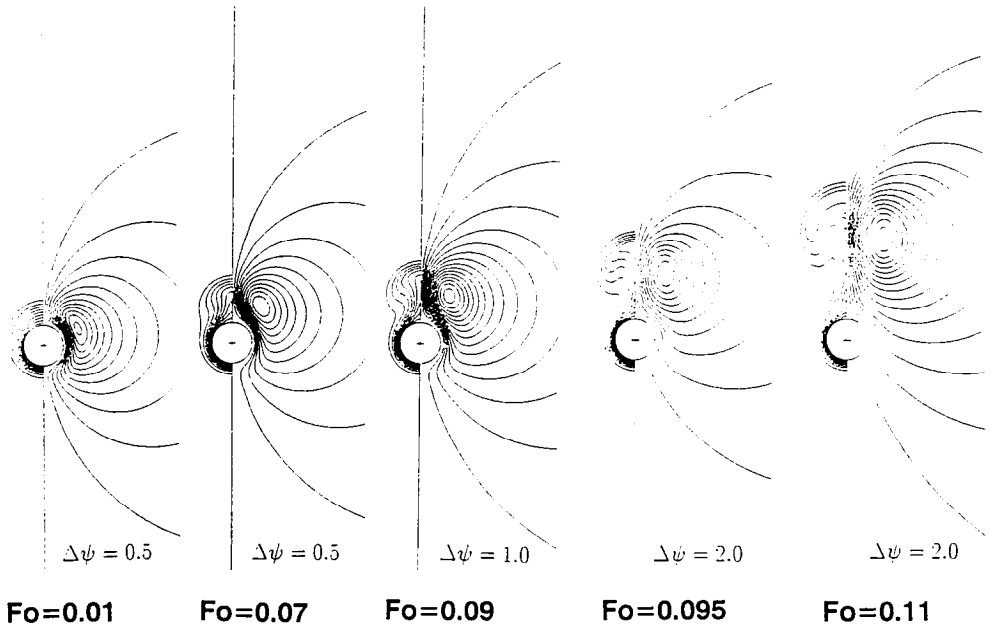


FIG. 6. Time sequences for isotherms and streamlines ($Ra = 10^4$, $Pr = 0.7$).

We hope that the present BMSs will be validated by making comparisons with precise experiments using high-accuracy measuring techniques.

## 5. CONCLUDING REMARKS

New bench mark solutions have been presented for the two-dimensional buoyancy driven flow of air around a horizontal circular cylinder with Prandtl number 0.7.

The following conclusions may be drawn from the present study.

(i) The bench mark solutions (local and average Nusselt numbers) were obtained for $Ra = 10^3$–$10^5$, under the uniform surface temperature condition.

(ii) The fourth-order multi-point finite difference method, together with the logarithmic coordinate transformation technique, is a suitable means to obtain the BMSs against which other solutions can be compared.

(iii) The inflow–outflow condition at the outer boundary condition used by Kuehn and Goldstein was checked by adopting the solid boundary condition at 1000–20 000$D$. As a consequence the inflow–

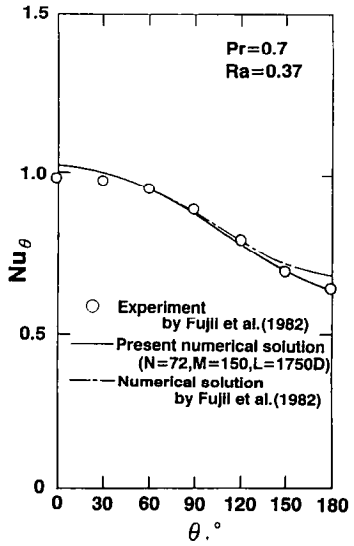


FIG. 7. Comparison of Nusselt numbers for $Ra = 0.37$ and $Pr = 0.7$ (Refs. [19, 20]).

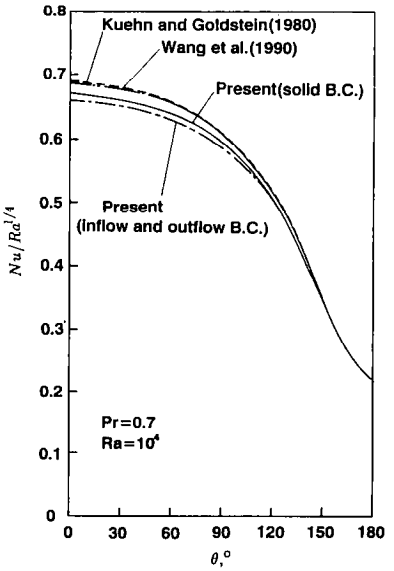


FIG. 8. Nusselt number comparison among four numerical solutions for $Ra = 10^4$ and $Pr = 0.7$.

Table 3. Local and average Nusselt numbers obtained by five finite difference schemes for $Ra = 10^5$ and $Pr = 0.7$

| Method | $Nu$ | | | | | | | $\overline{Nu}$ |
|---|---|---|---|---|---|---|---|---|
| | $\theta = 0$ | 30 | 60 | 90 | 120 | 150 | 180 | |
| EX-1 | 9.669 | 9.567 | 9.257 | 8.731 | 7.909 | 5.900 | 1.960 | 7.881 |
| ME-1 | 9.632 | 9.532 | 9.229 | 8.713 | 7.906 | 5.912 | 1.988 | 7.867 |
| ME-2 | 9.634 | 9.535 | 9.234 | 8.722 | 7.915 | 5.922 | 2.018 | 7.874 |
| ME-3 | 9.648 | 9.547 | 9.243 | 8.725 | 7.916 | 5.915 | 1.987 | 7.877 |
| ME-4 | 9.675 | 9.577 | 9.278 | 8.765 | 7.946 | 5.891 | 1.987 | 7.898 |

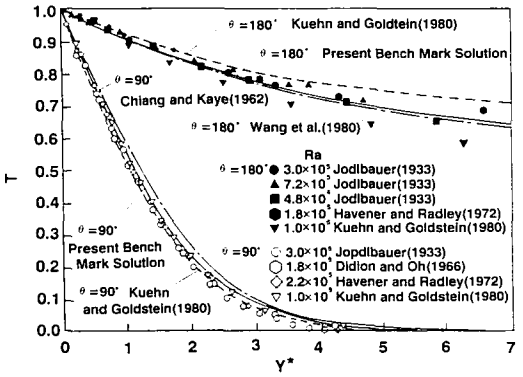


FIG. 9. Comparison between numerical solutions and experimental data for $Ra = 10^5$ and $Pr = 0.7$.

outflow condition gives a significant discrepancy compared with the solid boundary condition.

In closing, the authors hope that precise experiments will be done and their data compared with our BMSs in the near future.

## REFERENCES


1. T. H. Kuehn and R. J. Goldstein, Numerical solution to the Navier–Stokes equations for laminar natural convection about a horizontal isothermal circular cylinder, *Int. J. Heat Mass Transfer* **23,** 971–979 (1980).
2. J. H. Merkin, Free convection boundary layers on cylinders of elliptic cross section, *J. Heat Transfer* **99,** 453–457 (1977).
3. P. Wang, R. Kahawita and T. H. Nguyen, Numerical computation of the natural convection flow about a horizontal cylinder using splines, *Numer. Heat Transfer* **17A,** 191–215 (1990).
4. T. Fujii, M. Fujii and T. Honda, Theoretical and experimental study on free convection around a horizontal wire, *J. Soc. Mech. Engrs* **48**(431), 1312–1320 (1982).
5. T. Saitoh and K. Hirose, High-accuracy bench mark solutions to natural convection in a square cavity, *Comput. Mech.* **4,** 417–427 (1989).
6. G. de Vahl Davis, Natural convection of air in a square cavity: a bench mark numerical solution, *Int. J. Numer. Meth. Fluids* **3,** 249–264 (1983).
7. D. A. Didion and Y. H. Oh, A quantitative grid-schlieren method for temperature measurement in a free convection field, Technical Report No. 1, The Catholic University of America, Washington, DC (1966).
8. E. R. G. Eckert and E. E. Soehngen, Studies on heat transfer in laminar free convection with the Mach–Zehnder interferometer, Wright–Patterson AFB Technical Report (1948).
9. T. Saitoh, *Computer-aided Heat Transfer*. Youkendo, Tokyo (1986).
10. T. Aihara and E. Saito, Measurement of free convection velocity field around the periphery of a horizontal torus, *J. Heat Transfer* **94,** 95–98 (1972).
11. K. Jodbauer, Das Temperatur und Geschwindigkeitsfelt um ein Geheiztes Rohr bei freier Konvektion, *ForschHft. Ver. dt. Ing.* **4,** 158–172 (1933).
12. G. Havener and R. J. Radlay, Jr, Quantitative measurements using dual hologram interferometry, Aerospace Research Laboratories Report 72-0085 (1972).
13. W. H. McAdams, *Heat Transmission*, 3rd edn, p. 176. McGraw-Hill, New York (1954).
14. D. C. Collis and M. J. Williams, A.R.L. Aero. Note, p. 140 (1954).
15. S. Goldstein, *Modern Developments in Fluid Dynamics*. Oxford University Press (1938).
16. S. Levy, Integral methods in natural convection flow, *J. Appl. Mech.* **22,** 515–522 (1955).
17. T. Chiang and J. Kaye, On laminar free convection from a horizontal cylinder, *Proc. Fourth National Congress of Applied Mechanics*, pp. 1213–1219 (1962).
18. L. Elliot, Free convection on a two-dimensional or axisymmetric body, *Q. J. Mech. Appl. Math.* **23,** 153–162 (1970).
19. T. Fujii, M. Takeuchi, M. Fujii, K. Suzaki and H. Uehara, Experiments on natural-convection heat transfer from the outer surface of a vertical cylinder to liquids, *Int. J. Heat Mass Transfer* **13,** 753–787 (1970).
20. T. Fujii, I. Morioka and H. Uehara, Buoyant plume above a horizontal line heat source, *Int. J. Heat Mass Transfer* **16,** 755–767 (1973).